Radiation Physics and Chemistry 216 (2024) 111439

Contents lists available at ScienceDirect

Radiation Physics and Chemistry

journal homepage: www.elsevier.com/locate/radphyschem

In-situ radiological classification and characterization methodology of activated cables in particle accelerators

Patrycja Dyrcz *, Angelo Infantino, Nabil Menaa, Safouane El-Idrissi, Christophe Tromel, Heinz Vincke

European Organization for Nuclear Research-CERN, Radiation Protection Group, Meyrin, 1211, Switzerland

ARTICLE INFO

Keywords:
FLUKA
Activation
Material clearance
Fingerprint

ABSTRACT

The estimation of induced radioactivity and radiological classification of activated material is necessary throughout the life cycle of the Large Hadron Collider (LHC) accelerator. As part of the upgrade to High-Luminosity LHC (HL-LHC), radiation protection assessments need to be performed in order to estimate the radiological hazard during the dismantling activities of the LHC cables. The proposed In-situ radiological classification and characterization of the activated cables relies on validated FLUKA.CERN Monte Carlo simulations and analytical computations. The objective is to establish a methodology that allows clearing the material from regulatory control according to the Swiss Radiation Protection Legislation using the total gamma counting (TGC) analysis technique for an envelope set of activation scenarios. The study also includes a preliminary benchmark of the FLUKA geometry model and physics models based on gamma spectrometry laboratory analyses of representative samples.

1. Introduction

The High Luminosity Large Hadron Collider (HL-LHC) upgrade covers the decommissioning and removal of the LHC equipment and finally the installation of new machine components, mainly in the insertion regions (IR) IR1 and IR5 (around ATLAS and CMS experiments) (Aberle et al., 2020). The upgrade of the LHC to HL-LHC aims to increase the instantaneous luminosities by a factor of 5 from the LHC nominal value. The final upgrade to HL-LHC is foreseen in the Long Shutdown 3 (LS3), which will start in 2026 and will last for 3 years. One of the activities that need to be performed during LS3 is the removal of approximately 250 m^3 of cables (corresponding to 586 km) from IR1 and IR5 respectively.

During the LHC accelerator operational phase, cables within the machine tunnel are exposed to the shower of the scattered primary beam and secondary particles generated by the collisions, thus leading to induced radioactivity in the conductor and in the insulator material. For proper disposal of the cables, the estimations of induced radioactivity and radiological classification of activated material are necessary throughout the life cycle of the LHC.

With the HL-LHC upgrade, several radiation protection challenges need to be addressed concerning cable dismantling, transport and finally radiological characterization. In the context of radiological characterization, a preliminary phase so-called In-Situ characterization is investigated at first. It relies on FLUKA Monte Carlo simulations (FLUKA CERN, 2023; Ahdida et al., 2022; Battistoni et al., 2015), analytical computations using ActiWiz (Vincke and Theis, 2014), and Fluence Conversion Coefficient method (FCC) (Froeschl, 2018). Consequently, we developed a customized characterization methodology, prior to dismantling activities, based on total gamma counting (TGC) and the leading nuclide correlation method (LNC) associated with the conservative material nuclide vectors 'fingerprints' for activated cables in the LHC. The fingerprint is defined by maximizing the sum of Swiss clearance limits 'LL' (Limite de Libération) fractions per TGC signal. The methodology starts with the establishment of the radionuclide inventories and corresponding activity values for an appropriate range of activation scenarios (different cable material compositions, locations in the accelerator complex, and waiting times). Subsequently, the fingerprint, which corresponds to the scenario that yields the most conservative results is retained. The objective of the In-situ characterization is to predict the radionuclide inventory, estimate the specific activities, and establish the fingerprint for cable material type. It also aims at optimizing the cable removal process and minimizing the volume of the generated radioactive waste.

* Corresponding author.
E-mail address: patrycja.kinga.dyrcz@cern.ch (P. Dyrcz).

https://doi.org/10.1016/j.radphyschem.2023.111439
Received 5 November 2023; Accepted 28 November 2023
Available online 30 November 2023
0969-806X/© 2023 The Authors. Published by Elsevier Ltd. This is an open access article under the CC BY license (http://creativecommons.org/licenses/by/4.0/).

2. Materials and methods

2.1. Waste candidates and clearance criteria

One of the key parameters of radiological characterization of the activated cables is accurately determining the material chemical composition. On the other hand, thorough knowledge of the material composition is challenging due to the numerous cable types installed in the tunnel during the entire lifetime of the LHC accelerator.

The European Organization for Nuclear Research (CERN) Radiation Protection Group performed a study (Rimlinger et al., 2020) in order to indicate the representative cable families, namely (1) cables with aluminium wires and (2) cables with copper wires or both aluminium and copper wires. The chemical composition of these two cable families is based on the CERN catalogue of materials or X-ray Fluorescence (XRF) measurements on a number of cable samples. The retained composition is averaged over the different types of cables (i.a. power, signal and coaxial cables). It needs to be noted that the actual chemical composition of a given cable type may deviate from the reference one due to variations in the presence of trace elements. A third family of cable type, optical fibre, is also identified at CERN. The optical fibres are constituted of silica, $Si0_2$ (98 wt. %) with impurities of Fluorine (1 wt. %) and Chlorine (1 wt. %). Our investigations indicate that 75% of the optical fibre volume is the acrylate coating with no impurities. In addition to the removal of the cables, it is also planned to dismantle the cable support (cable-trays). The cable-trays installed in the LHC tunnel are typically made of steel (stainless steel 304L) or carbon steel. For the former material, the cobalt impurity is set to 0.1 wt% and for the latter to 0.005 wt% respectively.

Waste cable candidates, as described above, need to meet several criteria to be considered for clearance from the regulatory control in Switzerland. One of the criteria, as CERN adapted from The Swiss Federal Council (2018), indicates that each radionuclide's activity concentration cannot exceed the clearance limit, LL, expressed in Bq/g. In the case of a mix of radionuclides, the sum of LL fractions (LL_{SUM}) must be below unity, as presented in Eq. (1).

$$LL_{SUM} = \sum \frac{a_i}{LL_i} < 1, \tag{1}$$

where a_i is the specific activity of radionuclide i in a waste and LL_i represents the LL value for radionuclide i.

Also, the dose rate at 10 cm from the object's surface must be below 0.1 μSv/h, and the surface contamination must be below the surface contamination limits (CS) (The Swiss Federal Council, 2018) or, for a mixture of radionuclides, the sum of all ratios between the surface contamination (in Bq/cm^2) and the corresponding CS value must be below unit.

2.2. Radionuclide inventory prediction tools: FLUKA CERN, ActiWiz and FCC

In order to estimate the radionuclide inventory and the activity levels of the activated cables, Monte Carlo FLUKA.CERN (version 4.3-2) simulations were performed. The main source term considered was a symmetric proton–proton (pp) collision at 160 μrad half crossing angle, and $\sqrt{(s)}$ = 13.6 TeV centre-of-mass energy (i.e. 6.8 TeV per crossing beam) occurring at the Interaction Point 1 and 5 (IP1, IP5). The electromagnetic (EM) production and transport thresholds for the prompt simulation step are set to 1 MeV for e^+/e^- and 0.1 MeV for γ. Neutrons are transported down to thermal energies and the transport threshold for all other particles is set to 1 MeV. The applied irradiation profile covers the entire lifetime of the LHC accelerator until the end of 2025 (Run 3) (Elie et al., 2023).

The FLUKA simulations were used to compute the fluence spectra for neutrons, protons, photons, and charged pions (n, p, γ, π^+, π^-) for specific regions. Fig. 1 depicts the ten regions for which the fluence spectra were computed. The volume of each region filled with air was $20 \times 40 \times 100$ cm^3, in correspondence with existing cable-trays. The fluence spectra were incorporated into the analytical computation software ActiWiz Creator version 3.5 to generate radionuclide inventories and quantify the associated activity values.

In addition, the FCC values were applied via a dedicated user routine during the FLUKA radiation transport simulation. The FCC method is based on generating a set of particles (n, p, π^+, π^-) and energy-dependent coefficients for a given material composition, irradiation and waiting times, and for a scoring quantity, such as the sum of LL fractions. Consequently, the spatial maps were generated for the distribution of the LL_{SUM} in the LHC tunnel in Points 1 and 5 at the length of 270 m from the IP for 6 months and 1 year after the end of Run 3 pp operations.

2.3. Total gamma counting method and fingerprint selection

The method is based on total gamma counting (TGC) and the leading nuclide correlation method (LNC) associated with conservative fingerprints (Frosio et al., 2020; Harbron et al., 2023). The methodology starts with the establishment of the radionuclide inventory and the associated activity values for the considered activation scenarios in the LHC accelerator. It was performed using FLUKA simulations and ActiWiz computations. The former relied on scoring the fluence particle spectra by FLUKA USRTRACK card in the regions (see Fig. 1). The latter was based on constructing the activation scenarios for the computed fluence particle spectra. Each scenario assumed that the irradiation profile includes the entire lifetime of the LHC pp operation. The waiting times were 6 months 9 months, 1 year, 1.5 years and 2 years, according to the planned starting date of the cable removal works in the tunnel.

Afterwards, the most conservative fingerprint is established by maximizing the Figure Of Merit (FOM), given by Eq. (2).

$$FOM_j = \frac{LL_{SUM}}{TGC_{SIGNAL}} = \frac{\sum A_{i,j}/LL_i}{\sum A_{i,j} \times LNC_i}, \tag{2}$$

where FOM_j is the FOM for scenario j, $A_{i,j}$ represents the activity value of radionuclide i in scenario j. The LNC_i factor describes the detectability of a given radionuclide i in the TGC system, relative to Co-60.

For each material type, the radionuclide vectors were selected based on the scenarios yielding the highest FOM value for the associated waiting times and locations. The fingerprint is defined as the list of radionuclides needed to reach 90% (or 95%) of LL_{SUM} or TGC_{SIGNAL} respectively. Afterwards, the activity values for radionuclides that meet summation criteria (90% or 95% of LL_{SUM} or TGC_{SIGNAL}) were normalized to give 100% of the total specific activity value. It needs to be noted that the proposed fingerprints in the present paper can be deployed only for the TGC: RADOS RTM644,[1] from Mirion Technologies, serial number 40 as it incorporates the predicted TGC signal-specific response. However, the study can be extended to other types of TGC systems, accordingly.

2.4. Validation samples

In order to validate the radiation protection quantities provided by the FLUKA simulations, a quantitative comparison was performed. The analytical quantities given by FLUKA, such as activity values are compared with the corresponding set of gamma spectrometry (GS) measurements of the samples carried by a P-type High Purity Germanium detector from Mirion Technologies. The benchmark samples are made of aluminium and copper materials. They were installed in the LHC tunnel on the quadrupole magnets (the inner triplet). The samples were irradiated for a year during the LHC pp operation. The locations of the samples are shown in Fig. 1 along with the cable locations.

[1] https://www.mirion.com/products/rtm644inc-large-clearance-monitor last visited on 4 October 2023.

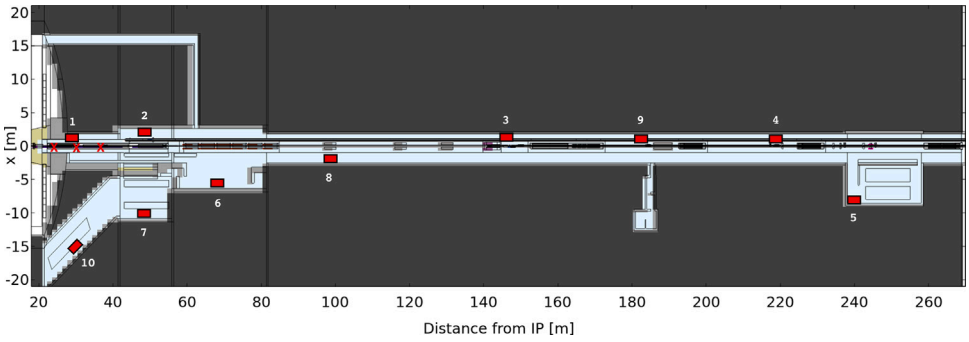

Fig. 1. The scheme of the cable fluence spectra calculation positions (red rectangles), and position for other benchmark aluminium and copper samples (red X) in the LHC tunnel in Point 1 right side.

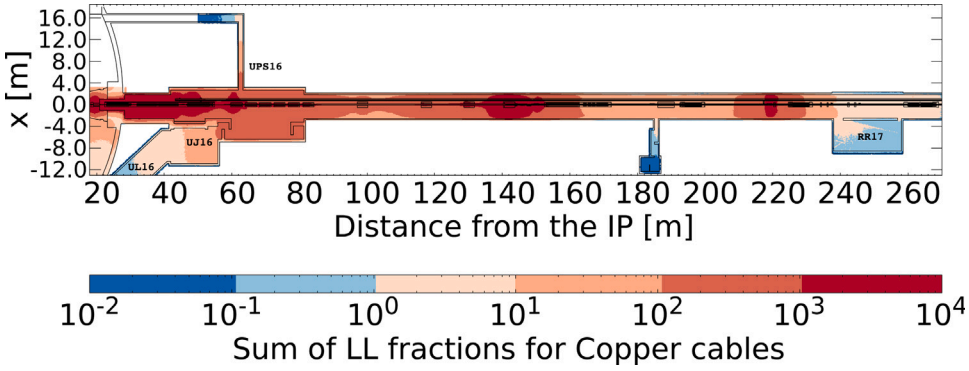

Fig. 2. Sum of LL fraction estimated for copper cables in Point 1 (average over Δy=± 150 cm at a height y = 50 cm) for 6 months after the end of Run 3 pp operation.

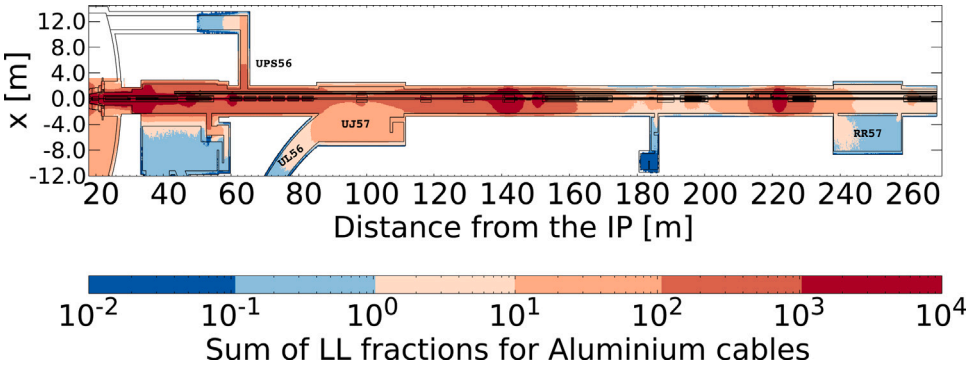

Fig. 3. Sum of LL fraction estimated for aluminium cables in Point 5 (average over Δy=± 150 cm at a height y = 50 cm) for 6 months after the end of Run 3 pp operation.

3. Results and discussion

3.1. Spatial distribution of the clearance hazard factor

The 2D maps of the clearance hazard factor were generated for the distribution of the LL_{SUM} for all considered cable and cable-tray materials, waiting times, and Point 1/Point 5 facilities. Figs. 2 and 3 show examples of the LL_{SUM} for copper and aluminium cables.

Point 1 map shows that the LL_{SUM} for the copper cables, installed along the LHC machine, is consistently above unity for a waiting time of 6 months after the end of Run 3 pp operation. The transition zone between non-radioactive and potentially radioactive copper cables appears to be in the service tunnel UL16. The 2D maps of Point 1 and Point 5 are similar for the copper and aluminium cables along the machine.

Point 5 map shows that the aluminium cables passing the UJ57 service tunnel are still radioactive after 6 months of waiting time. On the other side, in the RR57 area, the LL_{SUM} is below unity defining a clearance candidate region.

3.2. Radionuclide inventories and fingerprints

For each material type listed in Section 2.1 and waiting time value provided in Section 2.3, an activation scenario was generated using ActiWiz as described in 2.2. The output of this calculation is a list of radionuclides and associated specific activity values. As an example, Table 1 presents the top 10 contributors to the specific activity values for the most conservative activation scenario for carbon steel with a waiting time set to 1 year after the end of Run 3 pp operation (see Fig. 1, location 4). Furthermore, the process of computing the fingerprint in order to reach 90% (or 95%) to LL_{SUM} or TGC_{SIGNAL} is shown in Table 1 by indicating the surviving radionuclides after the 90% or 95% conditions.

Tables 2 and 3 present the conservative fingerprints for the TGC method for waiting times ranging from 6 months to 1 year, and from

Table 1
List of the top 10 radionuclides produced through activation of carbon steel located in the LHC tunnel for 1 year of waiting time.

Radionuclide	Activity (Bq/g)	LL (Bq/g)	LNC	fraction of LL_{SUM}	fraction of TGC_{SIGNAL}	Contribution to LL_{SUM} in %	Contribution to TGC_{SIGNAL} in %	Needed to reach 90% of LL_{SUM}	Needed to reach 90% of TGC_{SIGNAL}	Needed to reach 95% of LL_{SUM}	Needed to reach 95% of TGC_{SIGNAL}
Mn-54	38.19 (3.5%)	0.1	0.45321	381.86	17.31	92.99	85.60	Yes	Yes	Yes	Yes
Co-60	2.62 (1.9%)	0.1	1	26.22	2.62	6.38	12.94	No	Yes	Yes	Yes
Sc-46	0.08 (1%)	0.1	0.96909	0.83	0.08	0.20	0.40	No	No	No	No
Fe-55	286.31 (0.7%)	1000	0	0.29	0	0.07	0	No	No	No	No
Co-57	0.26 (2.4%)	1	0.01666	0.26	0.004	0.06	0.02	No	No	No	No
Fe-59	0.10 (4.6%)	1	0.50134	0.10	0.05	0.03	0.26	No	No	No	No
Co-58	0.08 (0.6%)	1	0.54174	0.08	0.04	0.02	0.21	No	No	No	No
H-3	1.57 (4.6%)	100	0	0.02	0	0.004	0	No	No	No	No
Ni-63	0.17 (0.9%)	100	0	0.002	0	0.0004	0	No	No	No	No
V-49	4.62 (1%)	10 000	0	0.0005	0	0.0001	0	No	No	No	No

Table 2
The most conservative fingerprints proposed for various waiting time ranges. The radionuclides contribute to 90% of LL_{SUM} or TGC_{SIGNAL}.

		90%	
Type	waiting time range	FOM	fingerprint (radionuclide, %Activity)
Copper cable	6 months – 1 year	11.9	Na-22, 2.2; Mn-54, 15.6; Co-56, 1.6; Co-57, 34.9; Co-58, 5.6; Co-60, 16.1; Zn-65, 7.5; Sb-124, 13.3; Sb-125, 3.4
Copper cable	1 year – 2 years	22.7	Co-60, 23.5; Zn-65, 46.8; Sb-125, 29.7
Aluminium cable	6 months – 1 year	12.8	Zn-65, 56.3; Sb-124, 43.7
Aluminium cable	1 year – 2 years	33.1	Na-22, 3.4; Zn-65 96.6
Optical fibre	6 months – 2 years	9.7	Na-22, 100
Carbon steel	6 months – 2 years	20.3	Mn-54, 93.6; Co-60, 6.4
Stainless steel 304	6 months – 2 years	12.9	Mn-54, 43.6; Co-60, 56.4

Table 3
The most conservative fingerprints proposed for various waiting time ranges. The radionuclides contribute to 95% of LL_{SUM} or TGC_{SIGNAL}.

		95%	
Type	waiting time range	FOM	fingerprint (radionuclide, %Activity)
Copper cable	6 months – 1 year	11.9	Na-22, 2.2; Mn-54, 15.6; Co-56, 1.6; Co-57, 34.9; Co-58, 5.6; Co-60, 16.1; Zn-65, 7.5; Sb-124, 13.3; Sb-125, 3.4
Copper cable	1 year – 2 years	22.7	Co-60, 22.7; Zn-65, 45.3; Sb-124, 3.2; Sb-125, 28.7
Aluminium cable	6 months – 1 year	12.8	Zn-65, 56.3; Sb-124, 43.7
Aluminium cable	1 year – 2 years	33.1	Na-22, 3.3; Zn-65 93.6; Sb-124, 3.1
Optical fibre	6 months – 2 years	9.7	Na-22, 100
Carbon steel	6 months – 2 years	20.3	Mn-54, 93.6; Co-60, 6.4
Stainless steel 304	6 months – 2 years	12.9	Mn-54, 35.6; Co-57, 16.9; Co-60, 46.1

Table 4
Activity comparison for the GS and FLUKA results. The activity uncertainties are quoted at 1 σ.

Sample material	Aluminium			Copper		
Radionuclide	Na-22			Co-60		
Sample position	FLUKA (Bq/g)	GS (Bq/g)	GS/FLUKA	FLUKA (Bq/g)	GS (Bq/g)	GS/FLUKA
P1-55-ITR	5.82 (1%)	3.29 (3%)	0.6 ± 0.05	1.62 (7%)	1.19 (4%)	0.7 ± 0.1
P1-56-ITR	5.03 (1%)	6.66 (15%)	1.3 ± 0.2	1.85 (4%)	2.68 (11%)	1.5 ± 0.2
P1-57-ITR	4.21 (1%)	2.49 (4%)	0.6 ± 0.05	1.46 (8%)	1.19 (4%)	0.8 ± 0.1

1 year to 2 years. The cable removal process is expected to start after 6 months from the end of Run 3 pp operations.

For copper cables, the highest contributing radionuclides to the fingerprint for a waiting time of 2 years are Zn-65, Sb-125 and Co-60. For aluminium cables, the contribution of the activity fraction of Zn-65 is increasing for longer waiting times. In the case of optical fibres, all the considered penalizing scenarios indicated that Na-22 is the only contributor to the fingerprint. For carbon steel and stainless steel 304L cable-trays the most conservative nuclide vector includes the radionuclides Mn-54 and Co-60 for waiting times ranging from 6 months to 2 years.

3.3. Validation of FLUKA CERN model

Table 4 presents a comparison of the activity values predicted by the FLUKA model and measured by GS for the aluminium and copper samples. The main gamma emitters are Na-22 in the aluminium samples and Co-60 in the copper samples. The reported uncertainty of the GS activity results does not include the systematic geometry model uncertainties due to the not well-known parameters.

The activity ratio of Na-22 ranges from 0.6 to 1.3 and for Co-60, it is between 0.7 and 1.5. Any discrepancies in the quantification of the included radioactivity between FLUKA simulations and GS sample measurements could be associated with the differences between the actual equipment geometry layout in the LHC tunnel and the FLUKA model. Nevertheless, the presented benchmark showed an agreement within a factor of 2 between the FLUKA model and GS measurement results. This consistency increases the confidence level one could assess the LL_{SUM} maps that are predicted by the FLUKA calculations. Future work includes continuing this validation effort on an annual basis as these samples can be accessed only once a year during the yearly shutdown period.

4. Conclusions

We have developed a radiological In-situ classification and characterization methodology of activated cables and associated cable trays in the LHC accelerator, which aims at clearing the material from the regulatory control according to the Swiss Radiation Protection Legislation. The methodology is based on the TGC analysis technique coupled with the conservative fingerprints for various activated cable types in the LHC tunnel (Points 1 and 5). The first phase of the methodology was to establish the radionuclide inventory and the associated specific activity values for all considered activation scenarios in the

LHC tunnel. For each material type, corresponding waiting times and ten specific regions, we computed the most conservative fingerprint by maximizing the FOM value. These fingerprints are useful during the future clearance campaigns that will be carried out on this material. It allows the optimization of the radioactive waste generation reducing the financial costs and the environmental impact of the CERN organization. Additionally, the LL_{SUM} maps were generated using the FCC method. It allows us to perform radiological zoning and precisely define the classification of the installed cables in the LHC tunnel (accelerator tunnel and service galleries) prior to dismantling. Furthermore, it points out where further sampling of the cables should be performed to optimize the cable removal works. Finally, the validation of the FLUKA model was carried out using high-energy resolution gamma spectrometry. The quantitative comparison showed that the specific activity values obtained by FLUKA simulations are consistent with the GS measurements of the aluminium and copper samples.

Declaration of competing interest

The authors declare that they have no known competing financial interests or personal relationships that could have appeared to influence the work reported in this paper.

Data availability

The authors do not have permission to share data.

References

Aberle, O., Béjar Alonso, I., Brüning, O., Fessia, P., Rossi, L., Tavian, L., Zerlauth, M., Adorisio, C., Adraktas, A., Ady, M., Albertone, J., Alberty, L., Alcaide Leon, M., Alekou, A., Alesini, D., Ferreira, B., Lopez, P., Ambrosio, G., Andreu Munoz, P., Anerella, M., Angal-Kalinin, D., Antoniou, F., Apollinari, G., Apollonio, A., Appleby, R., Arduini, G., Alonso, B., Artoos, K., Atieh, S., Auchmann, B., Badin, V., Baer, T., Baffari, D., Baglin, V., Bajko, M., Ball, A., Ballarino, A., Bally, S., Bampton, T., Banfi, D., Barlow, R., Barnes, M., Barranco, J., Barthelemy, L., Bartmann, W., Bartosik, H., Barzi, E., Battistin, M., Baudrenghien, P., Alonso, I., Belomestnykh, S., Benoit, A., Ben-Zvi, I., Bertarelli, A., Bertolasi, S., Bertone, C., Bertran, B., Bestmann, P., Biancacci, N., Bignami, A., Bliss, N., Boccard, C., Body, Y., Borburgh, J., Bordini, B., Borralho, F., Bossert, R., Bottura, L., Boucherie, A., Bozzi, R., Bracco, C., Bravin, E., Bregliozzi, G., Brett, D., Broche, A., Brodzinski, K., Broggi, F., Bruce, R., Brugger, M., Brüning, O., Buffat, X., Burkhardt, H., Burnet, J., Burov, A., Burt, G., Cabezas, R., Cai, Y., Calaga, R., Calatroni, S., Capatina, O., Capelli, T., Cardon, P., Carlier, E., Carra, F., Carvalho, A., Carver, L., Caspers, F., Cattenoz, G., Cerutti, F., Chancé, A., Rodrigues, M.C., Chemli, S., Cheng, D., Chiggiato, P., Chlachidze, G., Claudet, S., Coello De Portugal, J., Collazos, C., Corso, J., Costa Machado, S., Costa Pinto, P., Coulinge, E., Crouch, M., Cruikshank, P., Cruz Alaniz, E., Czech, M., Dahlerup-Petersen, K., Dalena, B., Daniluk, G., Danzeca, S., Day, H., De Carvalho Saraiva, J., De Luca, D., De Maria, R., De Rijk, G., De Silva, S., Dehning, B., Delayen, J., Deliege, Q., Delille, B., Delsaux, F., Denz, R., Devred, A., Dexter, A., Di Girolamo, B., Dietderich, D., Dilly, J., Doherty, A., Dos Santos, N., Drago, A., Drskovic, D., Ramos, D., Ducimetière, L., Efthymiopoulos, I., Einsweiler, K., Esposito, L., Esteban Muller, J., Evrard, S., Fabbricatore, P., Farinon, S., Fartoukh, S., Faus-Golfe, A., Favre, G., Felice, H., Feral, B., Ferlin, G., Ferracin, P., Ferrari, A., Ferreira, L., Fessia, P., Ficcadenti, L., Fiotakis, S., Fiscarelli, L., Fitterer, M., Fleiter, J., Foffano, G., Fol, E., Folch, R., Foraz, K., Foussat, A., Frankl, M., Frasciello, O., Fraser, M., Menendez, P., Fuchs, J., Furuseth, S., Gaddi, A., Gallilee, M., Gallo, A., Alia, R., Gavela, H., Matos, J., Garcia Morales, H., Valdivieso, A., Garino, C., Garion, C., Gascon, J., Gasnier, C., Gentini, L., Gentsos, C., Ghosh, A., Giacomel, L., Hernandez, K., Gibson, S., Ginburg, C., Giordano, F., Giovannozzi, M., Goddard, B., Gomes, P., Gonzalez De La Aleja Cabana, M., Goudket, P., Gousiou, E., Gradassi, P., Costa, A., Grand-Clément, L., Grillot, S., Guillaume, J., Guinchard, M., Hagen, P., Hakulinen, T., Hall, B., Hansen, J., Heredia Garcia, N., Herr, W., Herty, A., Hill, C., Hofer, M., Höfle, W., Holzer, B., Hopkins, S., Hrivnak, J., Iadarola, G., Infantino, A., Bermudez, S., Jakobsen, S., Jebramcik, M., Jenninger, B., Jensen, E., Jones, M., Jones, R., Jones, T., Jowett, J., Juchno, M., Julie, C., Junginger, T., Kain, V., Kaltchev, D., Karastathis, N., Kardasopoulos, P., Karppinen, M., Keintzel, J., Kersevan, R., Killing, F., Kirby, G., Korostelev, M., Kos, N., Kostoglou, S., Kozsar, I., Krasnov, A., Krave, S., Krzempek, L., Kuder, N., Kurtulus, A., Kwee-Hinzmann, R., Lackner, F., Lamont, M., Lamure, A., m, L., Lazzaroni, M., Le Garrec, M., Lechner, A., Lefevre, T., Leuxe, R., Li, K., Li, Z., Lindner, R., Lindstrom, B., Lingwood, C., Löffler, C., Lopez, C., Lopez-Hernandez, L., Losito, R., Maciariello, F., Macintosh, P., Maclean, E., Macpherson, A., Maesen, P., Magnier, C., Durand, H., Malina, L., Manfredi, M., Marcellini, F., Marchevsky, M., Maridor, S., Marinaro, G., Marinov, K., Markiewicz, T., Marsili, A., Martinez Urioz, P., Martino, M., Masi, A., Mastoridis, T., Mattelaer, P., May, A., Mazet, J., Mcilwraith, S., McIntosh, E., Medina Medrano, L., Mejica Rodriguez, A., Mendes, M., Menendez, P., Mensi, M., Mereghetti, A., Mergelkuhl, D., Mertens, T., Mether, L., Métral, E., Migliorati, M., Milanese, A., Minginette, P., Missiaen, D., Mitsuhashi, T., Modena, M., Mokhov, N., Molson, J., Monneret, E., Montesinos, E., Moron-Ballester, R., Morrone, M., Mostacci, A., Mounet, N., Moyret, P., Muffat, P., Muratori, B., Muttoni, Y., Nakamoto, T., Navarro-Tapia, M., Neupert, H., Nevay, L., Nicol, T., Nilsson, E., Ninin, P., Nobrega, A., Noels, C., Nolan, E., Nosochkov, Y., Nuiry, F., Oberli, L., Ogitsu, T., Ohmi, K., R. O., Oliveira, J., Orlandi, P., Ortega, P., Osborne, J., Otto, T., Palumbo, L., Papadopoulou, S., Papaphilippou, Y., Paraschou, K., Parente, C., Paret, S., Park, H., Parma, V., Pasquino, C., Patapenka, A., Patnaik, L., Pattalwar, S., Payet, J., Pechaud, G., Pellegrini, D., Pepinster, P., Perez, J., Espinos, J., Marcone, A., Perin, A., Perini, P., Persson, T., Peterson, T., Pieloni, T., Pigny, G., Pinheiro de Sousa, J., Pirotte, O., Plassard, F., Pojer, M., Pontercorvo, L., Poyet, A., Prelipcean, D., Prin, H., Principe, R., Pugnat, T., Qiang, J., Quaranta, E., Rafique, H., Rakhno, I., Duarte, D., Ratti, A., Ravaioli, E., Raymond, M., Redaelli, S., Renaglia, T., Ricci, D., Riddone, G., Rifflet, J., Rigutto, E., Rijoff, T., Rinaldesi, R., Riu Martinez, O., Rivkin, L., Rodriguez Mateos, F., Roesler, S., Romera Ramirez, I., Rossi, A., Rossi, L., Rude, V., Rumolo, G., Rutkovksi, J., Sabate Gilarte, M., Sabbi, G., Sahner, T., Salemme, R., Salvant, B., Galan, F., Santamaria Garcia, A., Santillana, I., Santini, C., Santos, O., Diaz, P., Sasaki, K., Savary, F., Sbrizzi, A., Schaumann, M., Scheuerlein, C., Schmalzle, J., Schmickler, H., Schmidt, R., Schoerling, D., Segreti, M., Serluca, M., Serrano, J., Sestak, J., Shaposhnikova, E., Shatilov, D., Siemko, A., Sisti, M., Sitko, M., Skarita, J., Skordis, E., Skoufaris, K., Skripka, G., Smekens, D., Sobiech, Z., Sosin, M., Sorbio, M., Soubelet, F., Spataro, B., Spiezia, G., Stancari, G., Staterao, M., Steckert, J., Steele, G., Sterbini, G., Struik, M., Sugano, M., Szeberenyi, A., Taborelli, M., Tambasco, C., Rego, R., Tavian, L., Teissandier, B., Templeton, N., Therasse, M., Thiesen, H., Thomas, E., Toader, A., Todesco, E., Tomás, R., Toral, F., Torres-Sanchez, R., Trad, G., Triantafyllou, N., Tropin, I., Tsinganis, A., Tuckamantel, J., Uythoven, J., Valishev, A., Van Der Veken, F., Van Weelderen, R., Vande Craen, A., Vazquez De Prada, B., Velotti, F., Verdu Andres, S., Verweij, A., Shetty, N., Vlachoudis, V., Volpini, G., Wagner, U., Wanderer, P., Wang, M., Wang, X., Wanzenberg, R., Wegscheider, A., Weisz, S., Welsch, C., Wendt, M., Wenninger, J., Weterings, W., White, S., Widuch, K., Will, A., Willering, G., Wollmann, D., Wolski, A., Wozniak, J., Wu, Q., Xiao, B., Xiao, L., Xu, Q., Yakovlev, Y., Yammine, S., Yang, Y., Yu, M., Zacharov, I., Zagorodnova, O., Zannini, C., Zanoni, C., Zerlauth, M., Zimmermann, F., Zlobin, A., Zobov, M., Zurbano Fernandez, I., 2020. High-Luminosity Large Hadron Collider (HL-LHC): Technical design report. In: CERN Yellow Reports: Monographs, CERN, Geneva, http://dx.doi.org/10.23731/CYRM-2020-0010, https://cds.cern.ch/record/2749422.

Ahdida, C., Bozzato, D., Calzolari, D., Cerutti, F., Charitonidis, N., Cimmino, A., Coronetti, A., D'Alessandro, G.L., Donadon Servelle, A., Esposito, L.S., Froeschl, R., García Alía, R., Gerbershagen, A., Gilardoni, S., Horváth, D., Hugo, G., Infantino, A., Kouskoura, V., Lechner, A., Lefebvre, B., Lerner, G., Magistris, M., Manousos, A., Moryc, G., Ogallar Ruiz, F., Pozzi, F., Prelipcean, D., Roesler, S., Rossi, R., Sabaté Gilarte, M., Salvat Pujol, F., Schoofs, P., Stránský, V., Theis, C., Tsinganis, A., Versaci, R., Vlachoudis, V., Waets, A., Widorski, M., 2022. New capabilities of the FLUKA multi-purpose code. Front. Phys. 9, http://dx.doi.org/10.3389/fphy.2021.788253, 788253. 14 p, URL https://cds.cern.ch/record/2806210.

Battistoni, G., et al., 2015. Overview of the FLUKA code. Ann. Nucl. Energy 82, 10–18. http://dx.doi.org/10.1016/j.anucene.2014.11.007.

Elie, L., Dyrcz, P., Infantino, A., Tromel, C., Vincke, H., 2023. Radiation protection challenges for the large hadron collider upgrade. Radiat. Prot. Dosim. 199 (8–9), 900–910. http://dx.doi.org/10.1093/rpd/ncad119, arXiv:https://academic.oup.com/rpd/article-pdf/199/8-9/900/50435583/ncad119.pdf.

FLUKA CERN, 2023. URL https://fluka.cern. (Accessed 16 August 2023).

Froeschl, R., 2018. A method for radiological characterization based on fluence conversion coefficients. J. Phys.: Conf. Ser. 1046, http://dx.doi.org/10.1088/1742-6596/1046/1/012006, 012006. 10 p, URL https://cds.cern.ch/record/2636326.

Frosio, T., Menaa, N., Dumont, G., Aberle, F., 2020. New methodology for in-situ classification of radiological items with a clearance monitor system. Nucl. Instrum. Methods Phys. Res. A 966, 163847. http://dx.doi.org/10.1016/j.nima.2020.163847, URL https://www.sciencedirect.com/science/article/pii/S0168900220303582.

Harbron, R., Charousset, R., Dumont, G., Magistris, M., Menaa, N., Giunio Pisano, P., Theis, C., 2023. Radiological characterisation for the clearance of burnable waste produced at CERN. Appl. Radiat. Isot. 196, 110782. http://dx.doi.org/10.1016/j.apradiso.2023.110782, URL https://www.sciencedirect.com/science/article/pii/S0969804323001355.

Rimlinger, M., Frosio, T., Menaa, N., Magistris, M., Theis, C., 2020. Qualification of gamma spectrometry measurement for the radiological characterization of mixed VLLW cables in particle accelerators. Appl. Radiat. Isot. 166, 109419. http://dx.doi.org/10.1016/j.apradiso.2020.109419, URL https://www.sciencedirect.com/science/article/pii/S0969804320305650.

The Swiss Federal Council, 2018. Ordonnance sur la radioprotection (ORaP) 814.501.

Vincke, H., Theis, C., 2014. ActiWiz – optimizing your nuclide inventory at proton accelerators with a computer code. In: Hirayama, H. (Ed.), Prog. Nucl. Sci. Tech. 4, 228–232. http://dx.doi.org/10.15669/pnst.4.228.